Computational and experimental studies of reactive intermediates in glycosylation reactions

Remmerswaal, W.A.

Chapter 10

Summary and Perspectives

Summary

Carbohydrates, or sugars, are the most diverse and most abundant biomolecules known. However, the isolation of carbohydrate samples in sufficient amounts and purity is often impractical or even impossible, so the chemical synthesis of glycosides becomes relevant. The glycosylation reaction, in which a glycosidic linkage is constructed from two glycosyl building blocks to form more complex (oligo)saccharides, is a central reaction in this endeavor. The most common approach to chemically create glycosidic bonds is a nucleophilic substitution reaction between a glycosyl electrophile (donor) carrying an anomeric leaving group, and a glycosyl acceptor containing a nucleophilic alcohol.

The principal challenge in forming glycosidic bonds by chemical means, is their stereoselective installation. The current view of the mechanism is described below (Figure 1). First an anomeric leaving group of a donor glycon is activated by a promotor (E-X), leading to an equilibrium of reactive intermediates. The stability and reactivity of these species strongly determine which intermediate acts as the dominant reactive intermediate. Covalent reactive intermediates provide more S_N2-like reactions, while more dissociated intermediates give rise to S_N1-like reactions. Although both S_N2- and S_N1-like reactions can give rise to both the α and β anomer, the stereoselectivity of these reactions is greatly determined by the nature of the reactive intermediates and the incoming nucleophile. The research described in this thesis aims to characterize reactive intermediates that dictate the stereoselectivity of glycosylation reactions.

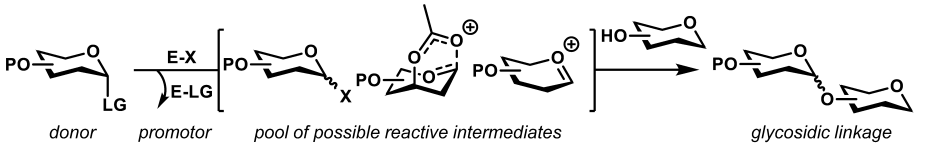

Figure 1. General overview of the glycosylation reaction.

Chapter 2 describes a computational approach to investigate additions of allyltrimethylsilane to mono-substituted pyranosyl oxocarbenium ions. These reactions preferentially proceed following a reaction path where the oxocarbenium ion transforms from a half chair ($^3H_4$ or $^4H_3$) to a chair conformation (Figure 1a). The activation strain model is used to quantify important steric and electronic interactions and structural features that occur in the transition states of the reactions to understand the relative energy barriers of the diastereotopic addition reactions. Overall, the stereoselectivity in the reactions closely matches the "intrinsic preference" of the cations, as dictated by the stability of individual half chair conformers. However, for the C5-CH_2OMe substituent, steric factors override the "intrinsic preference", leading to a more selective reaction than would be expected based on the preferred shape of the ion (Figure 1b).

Chapter 3 expands on Chapter 2 by applying this methodology to oxocarbenium ions formed from glucosyl and mannosyl donors. A computational approach is used to rationalize the experimental outcome obtained with a pair of weak *C*-nucleophiles. It is established that the S_E2' reactions of fully substituted carbohydrates do not always proceed through chair-like transition states. Notably, the formation of the α-products from the mannosyl cation is the result of an addition reaction to a boat-like conformer. Quantum chemical analyses highlight the physical factors responsible for the unexpected twist boat-like transition state, which is favored over a chair-like transition state, because the latter experiences increased steric hindrance (Figure 1c).

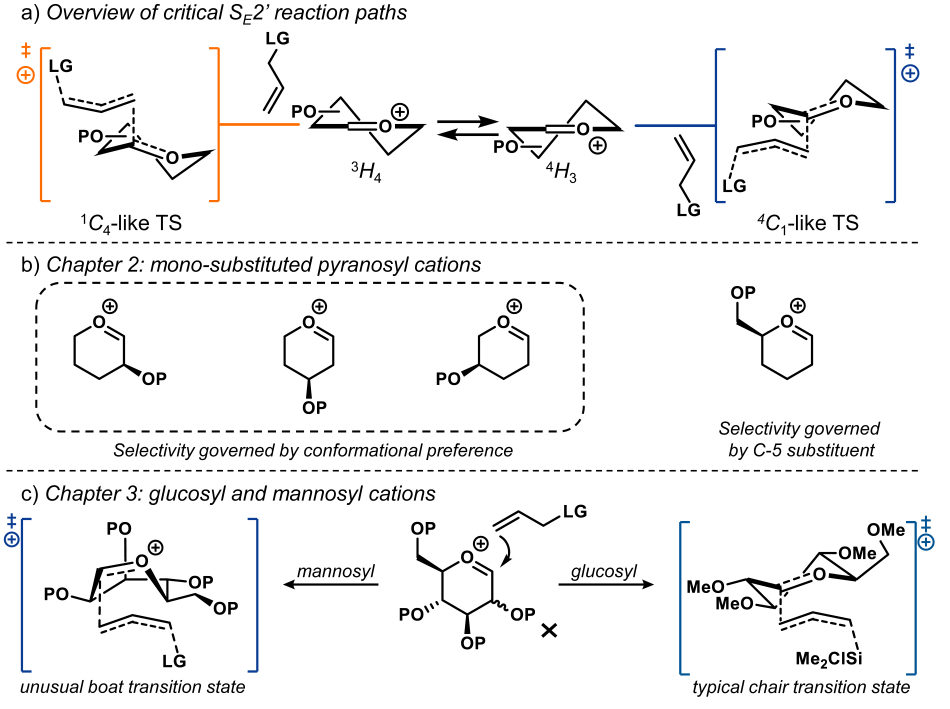

Figure 2. a) Glycosylations with allylic *C*-nucleophiles occur following S_E2' reaction paths, of which $^1C_4$ and $^4C_1$-like transition states are generally the most relevant. b) Chapter 2 focusses on the S_E2' reactions of mono-substituted pyranosyl cations. c) Chapter 3 focusses on the S_E2' reactions of fully substituted pyranosyl cations, which may access unusual skew-boat like transition states.

Chapter 4 examines neighboring-group participation by C-2 acyloxy groups. A single acyloxy group at C-2 can control the outcome of nucleophilic substitution reactions of pyran-derived acetals, but the extent of the neighboring-group participation depends on a number of factors. This chapter establishes that the 1,2-*trans* selectivity increases with increasing reactivity of the nucleophile and the electron withdrawing character of the acyloxy group. Computational studies show a strong correlation between these factors and the barriers for the ring-opening reaction on the dioxolenium ions (Figure 3).

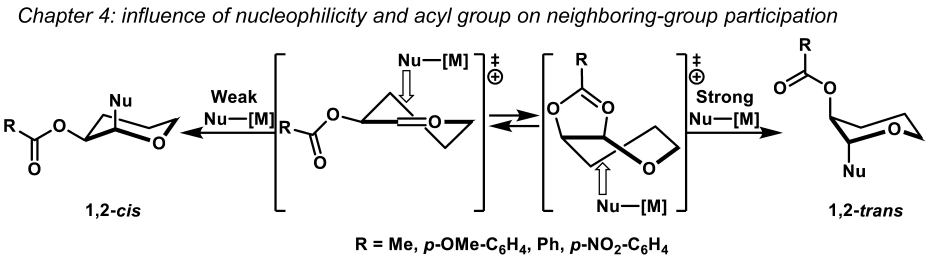

Figure 3. Chapter 4 examines neighboring-group participation by C-2 acyloxy groups.

Chapter 5 Investigates long-range participation (LRP). While neighboring-group participation provides 1,2-*trans* glycosides, long-range participation (LRP) of acyl groups from distal positions (*i.e.*, C-3, C-4, and C-6) can enable the introduction of 1,2-*cis* linkages (Figure 4a). It has been reported that the 2,2-dimethyl-2-(*ortho*-nitrophenyl)acetyl (DMNPA) protecting group offers enhanced stereoselective steering compared to other acyl groups. In this chapter, the origin of the stereoselectivity induced by the DMNPA group is investigated through a systematic set of glycosylation reactions in combination with infrared ion spectroscopy (IRIS) to investigate the nature of the potentially formed glycosyl cations. This study indicates that the origin of the DMNPA stereoselectivity does not lie in the direct participation of the nitro moiety, but in the formation of a dioxolenium ion that is strongly stabilized by the nitro group (Figure 4b).

Chapter 6 describes competing intramolecular LRP stabilization of uronic acid cations by the C-5 carboxylic acid *versus* a C-4 acetyl group. The glycosyl cations are studied by a combination of computational chemistry and IRIS. It is revealed that a mixture of bridged ions is formed in which the mixture is driven towards the C-1,C-5 dioxolenium ion when the C-2,C-5-relationship is *cis*, and towards the formation of the C-1,C-4 dioxepanium ion when this relation is *trans* (Figure 4c). Isomer-population analysis and interconversion barrier computations show that the two bridged structures are not in dynamic equilibrium and that their ratio parallels the stability of the structures, as computed with density functional theory.

Chapter 7 further investigates LRP by investigating the contrasting behavior of glycosylation systems involving 3-*O*-benzoyl/benzyl benzylidene glucosyl and mannosyl donors. Here, a combination of systematic glycosylation reactions, the characterization of potential reactive intermediates, and in-depth computational studies is used to study the disparate behavior of these glycosylation systems. Evidence is provided for the intermediacy of benzylidene mannosyl 1,3-dioxanium ions, while the formation of the analogous 1,3-glucosyl dioxanium ions is thwarted by a prohibitively strong flagpole interaction of the C-2-substituent with the C-5-proton in moving towards the transition state in which the glucose ring adopts a $B_{2,5}$-conformation (Figure 4d).

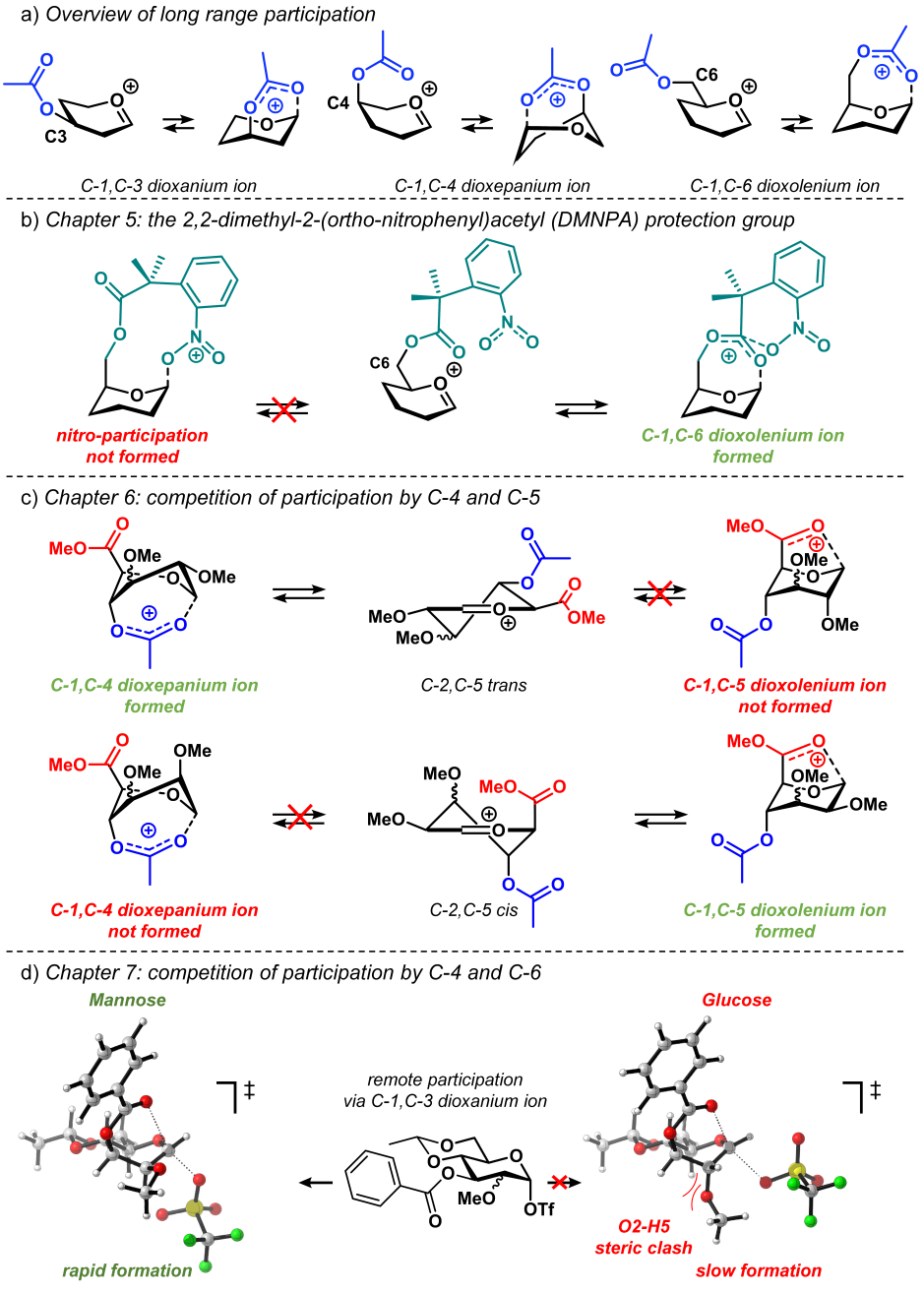

Figure 4. a) A general overview of long range participation (LRP). b) Chapter 5 investigates the reactive intermediates formed during reactions which employ the DMNPA protection group. c) Chapter 6 focusses on uronic acids carrying a C-4 acyl protecting group, and the resulting LRP competition between participation of C-4 and C-6. d) Chapter 7 investigates the disparate behavior of glycosylation systems involving 3-*O*-benzoyl benzylidene glucosyl and mannosyl donors.

Chapter 8 describes the influence of acceptor acidity on hydrogen bond mediated aglycone delivery (HAD) by the picoloyl protecting group. It is probed how the stereodirecting effect of the picoloyl protecting group depends on the acidity of the acceptor. To this end, a set of 3-*O*-functionalized glucosyl and mannosyl donors, each bearing different protecting groups (picolinate, nicotinate, isonicotinate, and benzoate), were synthesized for systematic evaluation. For the 3-*O*-picoloyl-glucose series, the picoloyl group exhibited minimal influence on stereoselectivity, with only weak nucleophiles showing a modest shift in selectivity for the 3-*O*-Pico protected glucosyl donor in comparison to the other C-3-acyl glucosides. In contrast, in the 3-*O*-picoloyl-mannose series, a stronger β-directing effect was observed, wherein more acidic acceptors led to increased β-selectivity.

Chapter 8: influence of acceptor acidity on hydrogen-bond-mediated aglycon delivery (HAD)

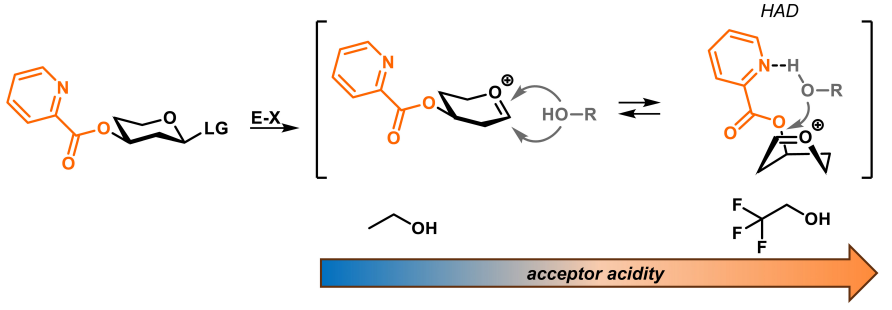

Figure 5. Chapter 8 elucidates the role of acceptor acidity on hydrogen-bond-mediated aglycon delivery (HAD) through the picoloyl protecting group.

Chapter 9 details a quantum chemical investigation into the intrinsic competition between the backside S_N2 (S_N2-b) and frontside S_N2 (S_N2-f) pathways using a set of simple alkyl triflate electrophiles in combination with a systematic series of phenol and partially fluorinated ethanol nucleophiles. It is shown how and why the well-established mechanistic preference for the S_N2-b pathway slowly erodes and can even be overruled by the unusual S_N2-f substitution mechanism along a series of strong to weak alcohol nucleophiles.

Chapter 9: backside versus frontside S_N2 reactions of alkyl triflates and alcohols

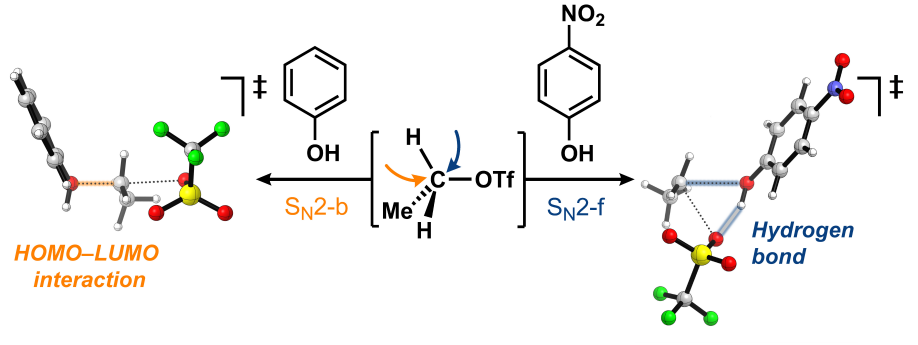

Figure 6. Chapter 9 covers the competition between backside and frontside S_N2 reactions of alkyl triflate electrophiles with alcohol nucleophiles.

To conclude, this thesis describes the use of experimental and computational chemistry to unravel the nature of reactive intermediates involved in the formation of glycosidic linkages. The research described here shows that glycosylation reactions can occur through various reactive intermediates, and the resulting pathways are often in competition. Characterization of these intermediates and the associated pathways aids in understanding the diastereomeric outcome of glycosylation reactions. It is shown how oxocarbenium ions can provide stereoselective reactions and how the stereoselectivity depends on the substituent pattern and nucleophilicity of the acceptor. Furthermore, it is examined how internal stabilization of oxocarbenium ions by neighboring and remote acyl protecting groups can provide stereoselectivity. The extent of this steering depends on the properties of the participating group, the nucleophilicity of the acceptor, and the configuration of the donor. In all, these studies provide novel insights that can be used to select better donor/acceptor combinations and glycosylation conditions, to steer the stereoselectivity of glycosylation reactions towards the desired product.

Future prospects

This thesis has explored glycosylation reactions involving different competing reactive intermediates. The main focus has been the computational characterization of the intermediates and their role in glycosylation reactions. It was observed that the stability and reactivity of the intermediates and the resulting glycosylation reaction pathways are strongly dependent on the configuration of the donor and the nucleophilicity of the acceptor. This section describes the initial findings of a study to extend the research presented in this thesis, expanding on the effect of the donor configuration and acceptor nucleophilicity. These initial investigations pave the way for further studies into glycosylation reactions employing more elaborate models and higher accuracy quantum mechanical methods.

The influence of acceptor reactivity and donor configuration on the stereoselective outcome of *C*-glycosylations reactions.

It has been observed that the stereoselective outcome of *C*-glycosylations reactions between glycosyl donors and allyltrimethylsilane is dependent on the configuration of the donor. When a glucosyl donor (**1**) is used, the α-product is formed exclusively (>98:2, α:β), while the corresponding mannosyl donor (**2**) provides a mixture of products (66:34 α:β).[1] The reactions with stronger *C*-nucleophiles, results in a shift towards formation of the β-product for both donors.[2] It has, for instance, been reported that reactions of allyltributylstannane and glucosyl and mannosyl sulfoxide donors provide mixtures of anomers.[3] The use of less reactive *C*-nucleophiles can also lead to a shift in the stereoselectivity of glycosylation reactions. In chapter 3, it was observed that the use of the weak *C*-nucleophile allyl(chloro)dimethylsilane did not lead to a change in the stereoselectivity for the reaction with glucosyl donor **1**, but that the stereoselectivity in the reaction of mannosyl donor **2** shifted to provide solely the α-product. Thus, the effect of the reactivity of the nucleophile depends on the configuration of the glycosyl donor.

To further investigate the influence of donor configuration on the stereochemical outcome of *C*-glycosylation reactions, a panel of eight phenyl 2,3,4,6-tetra-*O*-benzyl-1-thio-glycoside donors was generated, consisting of all possible hexopyranosyl configurations. The synthesis towards of of these eight donor configurations, *i.e.,* glucose, mannose, galactose, allose, altrose, gulose, idose and talose donors **1**-**8**, has been well-documented previously.[4–9] First, stereoselectivity-nucleophilicity trends of each donor were established through model glycosylations using a series of *C*-nucleophiles of gradually changing nucleophilicity. The *C*-nucleophiles used, in order of nucleophilicity as determined by the Mayr scale of reactivity, were: allyl(chloro)dimethylsilane (–0.57),[10] allyltrimethylsilane (1.68)[11] and allyltributylstannane (5.46).[12] Table 1 summarizes the observed stereoselectivity of the glycosylations of the eight glycosyl donors and these *C*-nucleophiles.[9]

All glycosylations employing the weakest nucleophile, allyl(chloro)dimethylsilane, were α-selective. Most donors, besides allose and gulose donors **4** and **6** (which provided the α-product exclusively), exhibited a shift towards β-selectivity as the nucleophilicity increased. The extent of this shift was observed to be configuration-dependent. Most notably, the donors exhibiting most β-selectivity (<50:50 α:β) carry an axial O-2 substituent (*i.e.,* mannose, altrose, idose, and talose donors **2**, **7,** and **8**). The effect of the other positions appears to be less pronounced. For instance, most donors possessing an axial O-4 (galactose, idose, and talose **3**, **7,** and **8**) provide somewhat more β-selective reactions than their equatorial O-4 counterparts (glucose, mannose and altrose **4**, **5,** and **10**, respectively). Altogether, besides position O-2, it is difficult to isolate a stereodirecting effect of a single position, and the stereoselectivity (or lack thereof) is the result of the interplay between the substituents.

Table 1. Glycosylation results with allyl(chloro)dimethylsilane, allyltrimethylsilane and allyltributylstannane under pre-activation conditions with Ph_2SO, Tf_2O. Ratio shown as α:β-ratio in which blue shows favoring α-selectivity and orange β-selectivity.

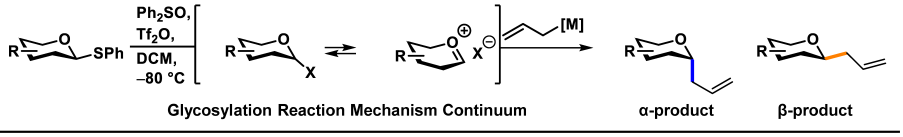

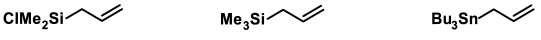

	Donor	Product α:β (yield)	Product α:β (yield)	Product α:β (yield)
1	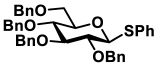	>98:2 [a] (58%)	>98:2 [a] (48%)	86:14 [a] (53%)
2		>98:2 (23%)	72:28 (66%)	28:72 (69%)
3	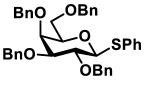	>98:2 (33%)	95:5 (46%)	40:60 (59%)
4	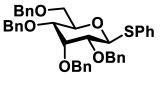	>98:2 (23%)	>98:2 (65%)	>98:2 (36%)
5	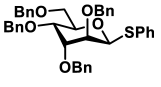	>98:2 (44%)	89:11 (53%)	57:43 (78%)
6	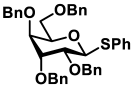	>98:2 (36%)	>98:2 (54%)	>98:2 (44%)
7	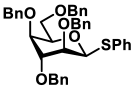	90:10 [b] (13%)	26:74 [b] (28%)	<2:98 [b] (23%)
8	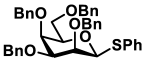	>98:2 (58%)	63:37 (37%)	18:82 (43%)

>90:10	>80:20	>60:40	50:50	<40:60	<20:80	<10:90	(α:β)

[a] Yield determined from inseparable α-thio-donor/product mixture. [b] Low yield is due to formation of the 1,6-anhydro-carbohydrate side product.

To understand the stereoselectivity of these glycosylation reactions, the computational methods developed in chapters 2 and 3 were applied.[13] In this method, the potential energy surface was examined, probing various possible S_E2' transition states leading to either the α or β-product. In chapter 3, five possible reaction pathways were identified. Three α-product-forming pathways: the bottom-face attack on a $^4H_3$-like conformer that proceeds through a $^4C_1$-like transition state; the bottom-face approach on a $^3H_4$-like conformer, leading to a $^3S_1$-like transition state; and a trajectory that involves bottom-face attack on a $B_{2,5}$-like conformation, leading to a $^0S_2$-like transition state. Furthermore, three possible β-product forming pathways were identified: a top-face attack on a $^3H_4$-conformation that passes through a $^1C_4$-shaped transition state, top-face attack on a $^4H_3$-like conformation through a $^1S_3$-slike transition state, and a top-face attack on a $B_{2,5}$-conformation through a $^1S_5$-shaped transition state (Table 2a). Here, these transition states for the corresponding glycosyl cations of donor **1**-**8** were computed, with allyl(chloro)dimethylsilane and allyltrimethylsilane as the nucleophile. Allyltributylstannane was excluded because no transition states could be identified due to the high reactivity of this nucleophile. Table 2b presents the S_E2' barriers of formation of the α- and β-products for the 2,6-*trans*-epimers (the gluco-, galacto-, allo- and gulosyl cations), while those for the 2,6-*cis*-epimers (the manno-, altro-, ido-, and tallosyl cations) are shown in Table 2c. Only the energies for the favored α- and β-product-forming pathways are given.

A global examination of the barriers shows that each glycosyl cation favors the formation of the α-product, independent of the nucleophile. These results are in line with the results from chapter 2 and 3, which indicate that steric interactions between the incoming nucleophile and the C5-CH_2OMe substituent provide a significant penalty for the β-product forming transition states. For the reactions with allyl(chloro)dimethyl silane, these activation energies correlate with the observed stereoselectivity of the glycosylations in Table 1. Increasing the reactivity of the nucleophile (allyltrimethylsilane) led to a decrease in barrier height for the formation of all products. Importantly, the trajectories followed for the formation of the α- and β-product did not change between both examined nucleophiles. Although all glycosyl cations still favored the α-product-forming itineraries, it was observed that the barriers for forming the β-product decreased more than those for forming the α-product. Likely, this difference is the result of the steric hindrance becoming less important as the transition states become earlier for the more reactive nucleophiles, leading to an increased distance between the nucleophile and the cation. The observed formation of anomeric mixtures when more reactive *C*-nucleophiles are used for the 2,6-*cis*-epimers (the manno-, altro-, ido- and tallosyl donors) likely results from the combination of oxocarbenium ions conformers that position the C-2 substituent in a *pseudo*-equatorial orientation, and overall lowering of the S_E2' barriers such that the $^1C_4$-like and $^1S_5$-like transition states become more favorable.

To fully understand the relationship between stereoselectivity, glycosyl donor configuration and acceptor reactivity, future computational studies must take into account the importance of counter-ions and the interconversion of the different oxocarbenium ion conformers. Including the counterion will bring a certain amount of S_N2-character to the substitution reactions, while significant energy barriers for the interconversion of oxocarbenium ion conformers can impede the accessibility of certain reaction pathways. In addition, the effect of the solvent on the reaction must be taken into account, for example, using DFT-based molecular dynamics approaches.[14]

Table 2. Gibbs free energies (in kcal mol^{-1})[a] of S_E2' transition states (a) originating from the favored α and β-product forming reaction pathways of b): glucosyl, galactosyl, allosyl, gulosy cations and c) mannosyl, altrosyl, idosyl, and talosyl (c) cations.

a)

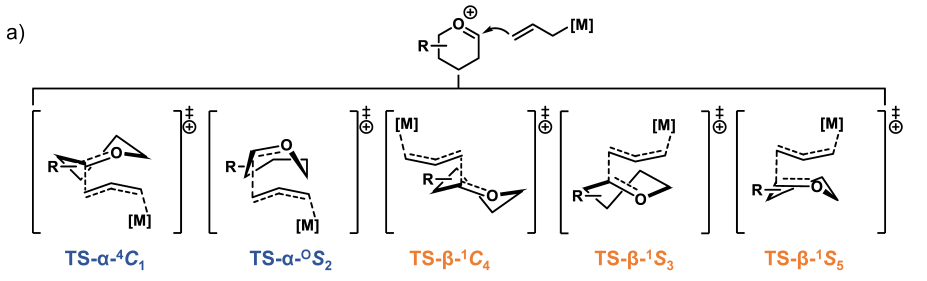

b)

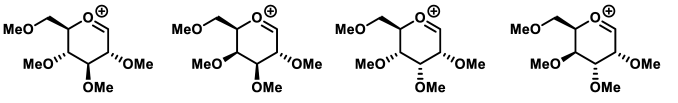

		Glucosyl	Galactosyl	Allosyl	Gulosyl
$ClMe_2Si$	β-TS	12.8 ($^1S_3$)	14.0 ($^1S_3$)	13.0 ($^1S_3$)	15.2 ($^1S_3$)
	α-TS	11.2 ($^4C_1$)	10.5 ($^4C_1$)	10.8 ($^4C_1$)	10.8 ($^4C_1$)
Me_3Si	β-TS	9.8 ($^1S_3$)	10.8 ($^1S_3$)	10.6 ($^1S_3$)	12.6 ($^1S_3$)
	α-TS	8.7 [b] ($^4C_1$)	7.7 [b] ($^4C_1$)	8.9 ($^4C_1$)	8.7 [b] ($^4C_1$)

c)

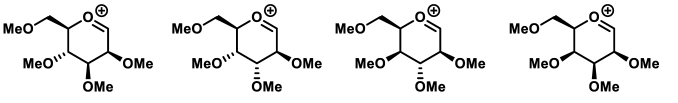

		Mannosyl	Altrosyl	Idosyl	Talosyl
$ClMe_2Si$	β-TS	13.0 ($^1C_4$)	13.1 ($^1C_4$)	14.0 ($^1S_5$)	14.8 ($^1S_5$)
	α-TS	10.8 [c] ($^OS_2$)	11.7 ($^4C_1$)	12.5 ($^4C_1$)	13.4 ($^4C_1$)
Me_3Si	β-TS	10.2 ($^1C_4$)	10.9 ($^1C_4$)	11.1[b] ($^1S_5$)	12.6 ($^1S_5$)
	α-TS	8.4 [c] ($^OS_2$)	9.0 [b] ($^4C_1$)	10.5 ($^4C_1$)	11.1 [b] ($^4C_1$)

[a] Gibbs free energies (T=213.15 K) were computed at the PCM(CH_2Cl_2)-B3LYP/6-311G(d,p) level of theory and are given relative to the separate reactants (the glycosyl cation and nucleophile). [b] As a transition state, the local maximum on the Gibbs free potential energy surface was used. The transition state could not be located due to instability of the associated reactant complex. [c] A representative structure for the transition state geometry was used.[15]

Supporting information

Computational methods

Using density functional theory (DFT), the potential energy surfaces (PES) of glycosyl cations were calculated. The DFT computations were performed using Gaussian 09 rev D.01.[16] For all computations, the hybrid functional B3LYP[17–19] and the 6-311G(d,p)[20] basis set were used. The geometry convergence criteria were set to tight (opt=tight; max. force=$1.5 \cdot 10^{-7}$, max. displacement=$6.0 \cdot 10^{-7}$), and an internally defined super-fine grid size was used (SCF=tight, int=veryfinegrid), which is a pruned 175,974 grid for first-row atoms and a 250,974 grid for all other atoms. These parameters were chosen as recent literature indicated a significant dependence of the computed frequencies on the molecule orientation when a smaller grid size is used.[21] Geometries were optimized without symmetry constraints. All calculated stationary points have been verified by performing a vibrational analysis, to be energy minima (no imaginary frequencies) or transition states (only one imaginary frequency). The character of the normal mode associated with the imaginary frequency of the transition state has been analyzed to ensure that it is associated with the reaction of interest. If a transition state could not be located, a constrained potential energy surface was constructed to estimate the barrier height.[13] Solvation in CH_2Cl_2 was taken into account in the computations using the PCM solvation model. Solvent effects were explicitly used in the solving of the SCF equations and during the optimization of the geometry and the vibrational analysis. The potential energy surfaces of the studied addition reactions were obtained by performing intrinsic reaction coordinate (IRC) calculations.

General experimental procedures

All chemicals (Acros, Fluka, Merck, and Sigma-Aldrich) were used as received unless stated otherwise. Dichloromethane was stored over activated 4 Å molecular sieves (beads, 8-12 mesh, Sigma-Aldrich). Before use traces of water present in the donor, diphenyl sulfoxide (Ph_2SO) and tri-*tert*-butylpyrimidine (TTBP) were removed by co-evaporation with dry toluene. The acceptors were stored in stock solutions (DCM, 0.5 M) over activated 3 Å molecular sieves (rods, size 1/16 in., Sigma-Aldrich). Trifluoromethanesulfonic anhydride (Tf_2O) was distilled over P_2O_5 and stored at –20 °C under a nitrogen atmosphere. Overnight temperature control was achieved by an FT902 Immersion Cooler (Julabo). Column chromatography was performed on silica gel 60 Å (0.04 – 0.063 mm, Screening Devices B.V.). TLC-analysis was conducted on TLC Silica gel 60 (Kieselgel 60 F_{254}, Merck) with UV detection by (254 nm) and by spraying with 20% sulfuric acid in ethanol followed by charring at ± 150 °C or by spraying with a solution of $(NH_4)_6Mo_7O_{24} \cdot H_2O$ (25 g/l) and $(NH_4)_4Ce(SO_4)4 \cdot {}_2H_2O$ (10 g/l) in 10% sulfuric acid in water followed by charring at ± 250 °C. High-resolution mass spectra were recorded on a Thermo Finnigan LTQ Orbitrap mass spectrometer equipped with an electrospray ion source in positive mode (source voltage 3.5 kV, sheath gas flow 10, capillary temperature 275 °C) with resolution R=60.000 at m/z=400 (mass range = 150-4000). ^1H and ^{13}C NMR spectra were recorded on a Bruker AV-400 NMR instrument (400 and 101 MHz respectively), a Bruker AV-500 NMR instrument (500 and 126 MHz respectively), or a Bruker AV-600 NMR instrument (600 and 151 MHz respectively). For samples measured in $CDCl_3$ chemical shifts (δ) are given in ppm relative to tetramethylsilane as an internal standard or the residual signal of the deuterated solvent. Coupling constants (*J*) are given in Hz. To get better resolution of signals with small coupling constants or overlapping signals a gaussian window function (LB ± -1 and GB ± 0.5) was used on the ^1H NMR spectrum. All given ^{13}C APT spectra are proton decoupled. NMR peak assignment was made using COSY, HSQC. If necessary additional NOESY, HMBC and HMBC-GATED experiments were used to elucidate the structure further. The anomeric product ratios were based on the integration of ^1H.

General glycosylation procedure: pre-activation Tf_2O/Ph_2SO based *C*-glycosylation.

A solution of the donor (100 µmol), Ph_2SO (26 mg, 130 µmol, 1.3 equiv) and TTBP (62 mg, 250 µmol, 2.5 equiv) in DCM (2 mL, 0.05 M) was stirred over activated 3 Å molecular sieves (rods, size 1/16 in., Sigma-Aldrich) for 30 min under an atmosphere of N_2. The solution was cooled to −80 °C and Tf_2O (22 µl, 130 µmol, 1.3 equiv) was slowly added to the reaction mixture. The reaction mixture was allowed to warm to −60 °C in approximately 45 min, followed by cooling to −80 °C and the addition of the acceptor (200 µmol, 2 equiv) in DCM (0.4 mL, 0.5 M). The reaction was allowed to warm up to −60 °C and stirred for an additional 18 h at this temperature until full reaction completion was observed. The reaction was quenched with sat. aq. $NaHCO_3$ at −60 °C and diluted with DCM (5 mL). The resulting solution was washed with H_2O and brine, dried over $MgSO_4$, filtered and concentrated under reduced pressure. Purification by column chromatography yielded the corresponding *C*-coupled glycoside.

Synthetic procedures of glycosylation products

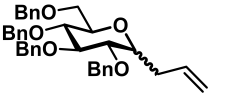

1-allyl-1-deoxy-2,3,4,6-tetra-*O*-benzyl-D-glucopyranoside (S1). The title compound was prepared according to the general glycosylation procedure, using glucose donor **1**[22] and allyl(chloro)dimethylsilane (0.058 mmol, 33 mg, 58%, >98:2, α:β) or allyltrimethylsilane (0.048 mmol, 27 mg, 48%, >98:2, α:β) or allyltributylstannane (0.053 mmol, 30 mg, 53%, 86:14, α:β), yielding the title compound as a colorless oil. Spectral data for the α-anomer: ^{1}H NMR (400 MHz, $CDCl_3$, HH-COSY, HSQC, HMBC, HMBC-GATED) δ 7.36 – 7.24 (m, 20H, CH_{Arom}), 5.81 (ddt, *J* = 17.2, 10.2, 6.8 Hz, 1H, CH_2-C*H*=CH_2), 5.14 – 5.03 (m, 2H, CH_2-CH=CH_2), 4.93 (d, *J* = 10.9 Hz, 1H, CH*H*Bn), 4.81 (dd, *J* = 10.8, 2.1 Hz, 2H, 2x CH*H*Bn), 4.72 – 4.59 (m, 3H, 3x CH*H*Bn), 4.51 – 4.41 (m, 2H, 2x CH*H*Bn), 4.13 (dt, *J* = 10.2, 5.1 Hz, 1H, H-1), 3.81 – 3.74 (m, 2H, H-2 H-3), 3.73 – 3.66 (m, 1H, H-6), 3.62 (m, 3H, H-4, H-5, H-6), 2.56 – 2.40 (m, 2H, CH_2-CH=CH_2). ^{13}C NMR (101 MHz, $CDCl_3$, HSQC, HMBC, HMBC-GATED) δ 138.9, 138.3, 138.29, 138.2 (C_q), 128.6, 128.6, 128.5, 128.3, 128.1, 128.1, 128.1, 128.0, 127.9, 127.1, 127.9, 127.8 (CH_{Arom}), 117.0 (CH_2-CH=CH_2), 82.5 (C-2 or C-3), 80.2 (C-2 or C-3), 78.2 (C-4 or C-5), 75.6, 75.2 (CHBn), 73.8 (C-1), 73.6, 73.2 (CHBn), 71.2 (C-4 or C-5), 69.0 (C-6), 29.9 (CH_2-C*H*=CH_2) HRMS (ESI) [M/Z]: [M + NH_4] calcd for $C_{37}NH_{44}O_5^+$ 582.3266 found 582.3217. β-anomer diagnostic peaks: ^{1}H NMR (400 MHz, $CDCl_3$, HH-COSY, HSQC, HMBC, HMBC-GATED) δ 5.99 – 5.88 (m, 1H, CH_2-C*H*=CH_2), 3.37 – 3.32 (m, 1H, H-1), 2.60 (dddd, *J* = 12.2, 6.1, 3.0, 1.4 Hz, 1H, CH_2-CH=CH*H*), 2.32 (dt, *J* = 14.2, 6.6 Hz, 1H). ^{13}C NMR (101 MHz, $CDCl_3$, HSQC, HMBC, HMBC-GATED) δ 134.9 (CH_2-*C*H=CH_2), 117.1 (CH_2-CH=*CH_2*), 87.4, 81.7, 79.1, 78.8, 78.7 (C-1), 75.7 (CH_2Bn), 75.1 (CH_2Bn), 69.1 (C-6), 36.1 (CH_2-CH=*CH_2*).

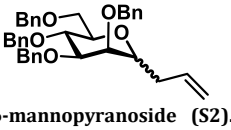

1-allyl-1-deoxy-2,3,4,6-tetra-*O*-benzyl-D-mannopyranoside (S2). The title compound was prepared according to the general glycosylation procedure, using mannose donor **2**[22] and allyl(chloro)dimethylsilane (0.023 mmol, 13 mg, 23%, >98:2, α:β) or allyltrimethylsilane (0.066 mmol, 37 mg, 66%, 72:28, α:β) or allyltributylstannane (0.069 mmol, 39 mg, 69%, 28:72, α:β), yielding the title compound as a colorless oil. Spectral data for the α-anomer: ^{1}H NMR (400 MHz, $CDCl_3$, HH-COSY, HSQC, HMBC, HMBC-GATED) δ 7.41 – 7.23 (m, 20H, CH_{Arom}), 5.81 – 5.69 (m, 1H, CH_2-C*H*=CH_2), 5.05 – 5.02 (m, 2H, CH_2-CH=CH_2), 4.72 (t, *J* = 5.9 Hz, 1H, CHBn), 4.63 – 4.50 (m, 7H, 7x CHBn), 4.09 – 4.01 (m, 1H, H-1), 3.85 (m, *J* = 6.1 Hz, 2H, H-4 H-5), 3.80 – 3.75 (m, 2H, H-6 H-3), 3.73 – 3.68 (m, 1H, H-6), 3.62 (dd, *J* = 4.6, 3.0 Hz, 1H, H-2), 2.39 – 2.26 (m, 2H, CH_2-CH=CH_2). ^{13}C NMR (101 MHz, $CDCl_3$, HSQC, HMBC, HMBC-GATED) δ 134.5 (CH_2-*C*H=CH_2), 128.5, 128.5, 128.5, 128.4, 128.2, 128.1, 128.0, 127.9, 127.8, 127.8 (CH_{Arom}), 117.3 (CH_2-*C*H=CH_2), 77.0 (C-3), 75.3 (C-2), 75.0 (C-4), 74.0 (CH-Bn), 73.8 (C-5), 73.4 (CH-Bn), 72.5 (C-1), 72.2 (CHBn), 71.6 (CHBn), 69.3 (C-6), 29.8 (*CH_2*-CH=CH_2). HRMS (ESI) [M/Z]: [M + NH_4] calcd for $C_{37}NH_{44}O_5^+$ 582.3266 found 582.3210. Spectral data for the β-anomer: ^{1}H NMR (400 MHz, $CDCl_3$, HH-COSY, HSQC, HMBC, HMBC-GATED) δ 7.54 – 7.16 (m, 20H, CH_{Arom}), 5.81 – 5.62 (m, 1H, CH_2-C*H*=CH_2), 5.07 – 4.98 (m, 2H, CH_2-CH=CH_2), 4.87 (d, *J* = 10.7 Hz, 1H, CH*H*Bn), 4.81 – 4.71 (m, 2H, 2x CH*H*Bn), 4.70 – 4.63 (m, 2H, 2x CH*H*Bn), 4.62 – 4.51 (m, 3H, 3x CH*H*Bn), 3.95 – 3.85 (m, 1H, H-4), 3.79 (td, *J* = 3.3, 1.4 Hz, 1H, H-2), 3.76 (dd, *J* = 4.4, 1.9 Hz, 1H, H-6), 3.74 – 3.65 (m, 1H, H-6), 3.61 (dd, *J* = 9.5, 2.8 Hz, 1H, H-3), 3.46 (ddd, *J* = 9.7, 5.9, 1.9 Hz, 1H, H-5), 3.36 – 3.31 (m, 1H, H-1), 2.51 (dtt, *J* = 14.3, 6.4, 1.6 Hz, 1H, CH*H*-CH=CH_2), 2.38 – 2.25 (m, 1H, CH*H*-CH=CH_2). ^{13}C NMR (101 MHz, $CDCl_3$, HSQC, HMBC, HMBC-GATED) δ 138.9, 138.6, 138.4 (C_q), 134.8 (*CH_2*-CH=CH_2), 128.5, 128.5, 128.5, 128.4, 128.4, 128.1, 128.0, 127.8, 127.8, 127.6, 127.6 (CH_{Arom}), 117.4 (CH_2-CH=*CH_2*), 85.6 (C-3), 80.0 (C-5), 78.4 (C-1), 75.6 (C-4), 75.4 (CH_2Bn), 74.7 (C-2), 74.4, 73.7, 72.6, 72.5 (CH_2Bn), 69.8 (C-6), 35.8 (*CH_2*-CH=CH_2). HRMS (ESI) [M/Z]: [M + NH_4] calcd for $C_{37}NH_{44}O_5^+$ 582.3266 found 582.3212.

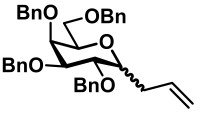

1-allyl-1-deoxy-2,3,4,6-tetra-*O*-benzyl-D-galactopyranoside (S3). The title compound was prepared according to the general glycosylation procedure, using galactose donor **3**[22] and allyl(chloro)dimethylsilane, yielding the title compound (0.033 mmol, 19 mg, 33%, >98:2, α:β) or allyltrimethylsilane (0.046 mmol, 26 mg, 46%, 95:5, α:β) or allyltributylstannane (0.059 mmol, 33 mg, 59%, 40:60, α:β), yielding the title compound as a colorless oil. Spectral data for the α-anozmer: ^{1}H NMR (400 MHz, $CDCl_3$, HH-COSY, HSQC, HMBC, HMBC-GATED) δ 7.35 – 7.25 (m, 20H, CH_{Arom}), 5.75 (ddt, *J* = 17.1, 10.2, 6.9 Hz, 1H, CH_2-C*H*=CH_2), 5.10 – 5.00 (m, 2H, CH_2-CH=CH_2), 4.70 (dd, *J* = 11.9, 2.6 Hz, 2H, 2x CH*H*Bn), 4.62 – 4.57 (m, 3H, 3x CH*H*Bn), 4.56 – 4.47 (m, 3H, C*H*HBn), 4.10 – 4.03 (m, 1H, H-5), 4.03 – 3.96 (m, 2H, H-1 H-3), 3.89 – 3.80 (m, 1H, H-6), 3.78 – 3.73 (m, 1H, H-4), 3.71 (dd, *J* = 6.8, 2.8 Hz, 1H, H-2), 3.66 (dd, *J* = 10.6, 4.6 Hz, 1H, H-6), 2.48 – 2.29 (m, 2H, CH_2-CH=CH_2). ^{13}C NMR (101 MHz, $CDCl_3$, HH-COSY, HSQC, HMBC, HMBC-GATED) δ 138.7, 138.6, 138.6, 138.4 ($C_{q\text{-}Arom}$), 135.3 (CH_2-CH=CH_2), 128.5, 128.5, 128.5, 128.4, 128.1, 128.0, 127.9, 127.9, 127.7, 127.7, 127.6 (CH_{Arom}), 116.9 (CH_2-*C*H=CH_2), 76.6 (C-4), 74.4 (C-3), 73.3, 73.2, 73.1 (CHBn), 72.3 (C-5 HSQC), 70.7 (C-1 HSQC), 67.4 (C-6), 29.8 (*CH_2*-CH=CH_2). HRMS (ESI) [M/Z]: [M + NH_4] calcd for $C_{37}NH_{44}O_5^+$ 582.3266 found 582.3220. Spectral data for the β-anomer: ^{1}H NMR (400 MHz, $CDCl_3$, HH-COSY, HSQC, HMBC, HMBC-GATED) δ 7.39 – 7.25 (m, 20H, CH_{Arom}), 5.91 (ddt, *J* = 17.1, 10.2, 6.8 Hz, 1H, CH_2-C*H*=CH_2), 5.13 – 5.00 (m, 2H, CH_2-*C*H=CH_2), 4.69 – 4.59 (m, 4H, 4x CH*H*Bn), 4.53 (dd, *J* = 13.7, 8.0 Hz, 2H, 2x CH*H*Bn), 4.44 (q, *J* = 11.8 Hz, 2H, 2x CH*H*Bn), 4.00 (dd, *J* = 4.0, 2.5 Hz, 1H, H-3), 3.74 – 3.71 (m, 1H, H-2), 3.61 (d, *J* = 2.8 Hz, 1H, H-4), 3.56 – 3.53 (m, 2H, H-6), 3.53 (s, 1H, H-5), 3.30 (ddd, *J* = 9.3, 8.2, 3.0 Hz, 1H, H-1), 2.60 (dddt, *J* = 14.7, 6.4, 3.1, 1.5 Hz, 1H, CH*H*-CH=CH_2), 2.37 – 2.26 (m, 1H, CH*H*-CH=CH_2). ^{13}C NMR (101 MHz, $CDCl_3$, HSQC, HMBC, HMBC-GATED) δ 138.9, 138.6, 138.2 (C_q), 135.4 (CH_2-*C*H=CH_2), 128.6, 128.5, 128.5, 128.2, 128.2, 127.9, 127.9, 127.9, 127.8, 127.7 (CH_{Arom}), 116.7 (CH_2-CH=*CH_2*), 85.0 (C-4), 79.5 (C-1), 78.7 (C-2), 77.3 (C-5), 75.5 (CH_2Bn), 74.5 (CH_2Bn), 73.8 (C-3), 73.6 (CH_2Bn), 72.3 (CH_2Bn), 69.2 (C-6), 36.3 (CH_2-CH=*CH_2*). HRMS (ESI) [M/Z]: [M + Na] calcd for $C_{37}H_{40}O_5Na^+$ 587.2776 found 587.2747.

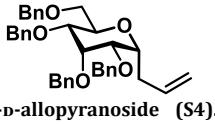

1-allyl-1-deoxy-2,3,4,6-tetra-*O*-benzyl-α-D-allopyranoside (S4). The title compound was prepared according to the general glycosylation procedure, using allose donor **4**[22] and allyl(chloro)dimethylsilane, yielding the title compound (0.023 mmol, 13 mg, 23%, >98:2, α:β) or allyltrimethylsilane (0.065 mmol, 37 mg, 65%, >98:2, α:β) or allyltributylstannane (0.036 mmol, 20 mg, 36%, >98:2, α:β), yielding the title compound as a colorless oil. ^{1}H NMR (400 MHz, $CDCl_3$, HH-COSY, HSQC, HMBC, HMBC-GATED) δ 7.38 – 7.26 (m, 20H, CH_{Arom}), 5.93 – 5.80 (m, 1H, CH_2-C*H*=CH_2), 5.11 – 4.99 (m, 2H, CH_2-CH=CH_2), 4.82 (d, *J* = 3.4 Hz, 2H, CHBn), 4.62 (d, *J* = 12.2 Hz, 1H, CHBn), 4.56 (s, 2H, 2x CHBn), 4.52 – 4.45 (m, 2H, 2x CHBn), 4.38 (d, *J* = 11.4 Hz, 1H, CHBn), 4.21 (t, *J* = 2.8 Hz, 1H, H-3), 4.11 (ddd, *J* = 11.3, 6.0, 3.1 Hz, 1H, H-1), 4.00 (ddd, *J* = 9.6, 3.5, 2.2 Hz, 1H, H-5), 3.76 (dd, *J* = 10.4, 3.5 Hz, 1H, H-6), 3.67 (dd, *J* = 10.5, 2.1 Hz, 1H, H-6), 3.62 (dd, *J* = 6.0, 2.6 Hz, 1H, H-2), 3.56 (dd, *J* = 9.7, 2.8 Hz, 1H, H-4), 3.05 (ddd, *J* = 15.7, 11.2, 7.5 Hz, 1H, CH_2-CH=CH*H*), 2.54 (dddd, *J* = 15.6, 6.3, 3.1, 1.5 Hz, 1H, CH_2-CH=C*H*H). ^{13}C NMR (101 MHz, $CDCl_3$, HSQC, HMBC, HMBC-GATED) δ 136.8 (CH_2-*C*H=CH_2), 128.6, 128.5, 128.4, 128.3, 128.0, 127.9, 127.9, 127.8, 127.8, 127.7, 127.5, 127.4 (CH_{Arom}), 116.3 (CH_2-CH=*CH_2*), 76.8 (C-2), 75.15 (C-4), 74.53 (C-1), 74.27 (C-3), 74.1, 73.7, 71.4, 71.4 (CH-Bn), 69.4 (C-6), 67.2 (C-5), 31.6 (*CH_2*-CH=CH_2). HRMS (ESI) [M/Z]: [M + Na] calcd for $C_{37}H_{40}O_5Na^+$ 587.2776 found 587.2768.

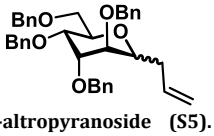

1-allyl-1-deoxy-2,3,4,6-tetra-*O*-benzyl-D-altropyranoside (S5). The title compound was prepared according to the general glycosylation procedure, using gulose donor **5**[22] and allyl(chloro)dimethylsilane (0.044 mmol, 25 mg, 44%, >98:2, α:β) or allyltrimethylsilane (0.053 mmol, 30 mg, 53%, 89:11, α:β) or allyltributylstannane (0.078 mmol, 44 mg, 78%, 57:43, α:β), yielding the title compound as a colorless oil. Spectral data for the α-anomer: ^{1}H NMR (400 MHz, $CDCl_3$, HH-COSY, HSQC, HMBC, HMBC-GATED) δ 7.39 – 7.23 (m, 20H, CH_{Arom}), 5.85 (ddt, *J* = 17.1, 10.2, 6.9 Hz, 1H, CH_2-C*H*=CH_2), 5.13 – 5.02 (m, 2H, CH_2-CH=CH_2), 4.68 (d, *J* = 11.4 Hz, 1H, CH*H*Bn), 4.57 (dd, *J* = 3.0, 1.6 Hz, 3H, 3x CH*H*Bn), 4.55 – 4.47 (m, 4H, 4x CH*H*Bn), 4.17 (q, *J* = 5.2 Hz, 1H, H-5), 3.86 (dd, *J* = 5.3, 3.2 Hz, 1H, H-4), 3.75 (dd, *J* = 6.6, 3.1 Hz, 1H, H-3), 3.73 – 3.69 (m, 1H, H-1), 3.66 – 3.61 (m, 2H, H-6 H-2), 3.58 (dd, *J* = 10.3, 4.8 Hz, 1H, H-6), 2.62 – 2.43 (m, 2H, CH_2-CH=CH_2). ^{13}C NMR (101 MHz, $CDCl_3$, HSQC, HMBC, HMBC-GATED) δ 138.5, 138.4, 138.3 (C_q), 135.3 (CH_2-*C*H=CH_2), 128.5, 128.4, 128.4, 128.2, 128.1, 128.0, 127.8, 127.8, 127.8, 127.7 (CH_{Arom}), 117.0 (CH_2-CH=*CH_2*), 77.4 (C-2/C-3), 77.3 (C-2/C-3), 74.8 (C-1), 73.5 (CH_2Bn), 73.5 (C-3), 72.2 (CH_2Bn) , 71.8 (C-5 CH_2Bn), 69.1 (C-6), 35.9 (*CH_2*-CH=CH_2). HRMS (ESI) [M/Z]:

[M + NH_4] calcd for $C_{37}NH_{44}O_5^+$ 582.3266 found 582.32204. Spectral data for the β-anomer: ^{1}H NMR (400 MHz, $CDCl_3$) δ 7.39 – 7.20 (m, 20H, CH_{Arom}), 5.68 (dddd, *J* = 17.1, 10.1, 8.0, 6.1 Hz, 1H, CH_2-C*H*=CH_2), 4.74 – 4.32 (m, 8H, CH_2Bn), 3.97 (ddt, *J* = 9.0, 5.8, 1.7 Hz, 1H, H-5), 3.80 (dd, *J* = 6.7, 1.6 Hz, 1H, H-1), 3.77 – 3.75 (m, 1H, H-6), 3.74 – 3.72 (m, 2H, H-3 H-4), 3.64 – 3.62 (m, 1H, H-6), 3.32 (dd, *J* = 3.5, 1.5 Hz, 1H, H-2), 2.48 – 2.41 (m, 1H, CH*H*-CH=CH_2), 2.34 – 2.20 (m, 1H, CH*H*-CH=CH_2). ^{13}C NMR (101 MHz, $CDCl_3$, HSQC, HMBC, HMBC-GATED) δ 138.8, 138.7, 138.5 (C_q), 135.1 (CH_2-*C*H=CH_2), 128.5, 128.5, 128.4, 128.4, 128.3, 128.3, 128.2, 128.1, 128.1, 128.0, 128.0, 127.9, 127.8, 127.8, 127.8, 127.7, 127.7, 127.5 (CH_{Arom}), 76.0 (C-2), 75.2 (C-1), 74.4 (C-3/C-4), 73.7, 73.6, 73.0, 72.7 (CH_2Bn), 70.2 (C-6). HRMS (ESI) [M/Z]: [M + Na] calcd for $C_{37}H_{40}O_5Na^+$ 587.2776 found 587.27669.

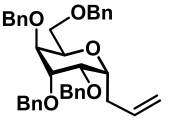

1-allyl-1-deoxy-2,3,4,6-tetra-*O*-benzyl-α-D-gulopyranoside (S6). The title compound was prepared according to the general glycosylation procedure, using gulose donor **6**[22] and allyl(chloro)dimethylsilane (0.036 mmol, 20 mg, 36%, >98:2, α:β) or allyltrimethylsilane (0.054 mmol, 30 mg, 54%, >98:2, α:β) or allyltributylstannane (0.044 mmol, 25 mg, 44%, >98:2, α:β), yielding the title compound as a colorless oil. ^{1}H NMR (400 MHz, $CDCl_3$, HH-COSY, HSQC, HMBC, HMBC-GATED) δ 7.48 – 7.43 (m, 2H, CH_{Arom}), 7.39 – 7.26 (m, 18H, CH_{Arom}), 5.78 (ddt, *J* = 17.1, 10.1, 6.9 Hz, 1H, CH_2-C*H*=CH_2), 5.10 – 5.04 (m, 1H, CH-C*H*=CH*H*), 5.01 (ddt, *J* = 10.2, 2.2, 1.1 Hz, 1H, CH-C*H*=CH*H*), 4.80 (d, *J* = 12.0 Hz, 1H, CH*H*Bn), 4.77 – 4.75 (m, 1H, CH*H*Bn), 4.73 (t, *J* = 6.5 Hz, 1H, CH*H*Bn), 4.69 – 4.65 (m, 2H, 2x CH*H*Bn), 4.59 – 4.55 (m, 2H, 2x CH*H*Bn), 4.54 – 4.50 (m, 2H, 2x CH*H*Bn), 4.22 (dt, *J* = 6.7, 4.8 Hz, 1H, H-5), 3.94 – 3.87 (m, 2H, H-1 H-4), 3.85 (t, *J* = 3.4 Hz, 1H, H-3), 3.79 (dd, *J* = 6.8, 3.0 Hz, 1H, H-2), 3.70 – 3.65 (m, 2H, 2x H-6), 2.73 (dt, *J* = 15.7, 8.0 Hz, 1H, CH*H*-CH=CH_2), 2.36 (dddd, *J* = 13.5, 7.2, 5.7, 3.1 Hz, 1H, CH*H*-CH=CH_2). ^{13}C NMR (101 MHz, $CDCl_3$, HSQC, HMBC, HMBC-GATED) δ 138.8, 138.7, 138.5 (C_q), 135.9 (CH_2-*C*H=CH_2), 131.2, 128.6, 128.5, 128.5, 128.5, 128.4, 128.3, 128.3, 128.1, 128.0, 128.0, 127.9, 127.9, 127.8, 127.8, 127.7, 127.7, 127.6, 127.6 (CH_{Arom}), 116.67 (CH_2-CH=*CH_2*), 77.7 (C-2), 75.9 (C-4), 75.1 (C-3), 73.7 (C-1), 73.5, 73.4, 73.1, 72.8 (CH_2Bn), 68.2 (C-6), 33.4 (*CH_2*-CH=CH_2). HRMS (ESI) [M/Z]: [M + NH_4] calcd for $C_{37}NH_{44}O_5^+$ 582.3266 found 582.3216.

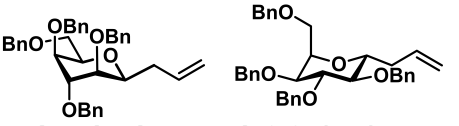

1-allyl-1-deoxy-2,3,4,6-tetra-*O*-benzyl-D-idopyranoside (S7). The title compound was prepared according to the general glycosylation procedure, using idose donor **7**[22] and allyl(chloro)dimethylsilane (0.013 mmol, 7 mg, 13%, 90:10, α:β) allyltrimethylsilane (0.028 mmol, 16 mg, 28%, 26:27, α:β) or allyltributylstannane yielded the title compound (0.023 mmol, 13 mg, 23%, 2:>98, α:β), yielding the title compound as a colorless oil. Spectral data for the α-anomer: ^{1}H NMR (600 MHz, $CDCl_3$, HH-COSY, HSQC, HMBC, HMBC-GATED) δ 7.37 – 7.26 (m, 20H, CH_{Arom}), 5.88 (dddd, *J* = 17.6, 10.3, 7.5, 6.2 Hz, 1H, CH_2-C*H*=CH_2), 5.13 – 5.04 (m, 2H, CH_2-CH=CH_2), 4.86 (dd, *J* = 12.2, 10.9 Hz, 2H, 2x CH*H*Bn), 4.73 (d, *J* = 11.0 Hz, 1H, 2x CH*H*Bn), 4.66 (d, *J* = 11.5 Hz, 1H, CH*H*Bn), 4.61 (dd, *J* = 11.2, 5.2 Hz, 2H, 2x CH*H*Bn), 4.57 (s, 2H, 2x CH*H*Bn), 4.23 (ddd, *J* = 8.6, 5.9, 3.3 Hz, 1H, H-5), 3.83 (dd, *J* = 11.0, 8.2 Hz, 1H, H-6), 3.80 – 3.73 (m, 1H, H-4), 3.74 – 3.72 (m, 2H, H-6 H-3), 3.72 – 3.70 (m, 1H, H-1), 3.26 (dd, *J* = 9.4, 8.1 Hz, 1H, H-2) 2.57 (dddt, *J* = 14.8, 6.4, 3.3, 1.5 Hz, 1H, CH*H*-CH=CH_2), 2.30 – 2.23 (m, 1H, CH*H*-CH=CH_2). ^{13}C NMR (151 MHz, $CDCl_3$, HH-COSY, HSQC, HMBC, HMBC-GATED) δ 138.8), 138.4, 138.4, 138.2 (C_q), 134.9 (CH_2-*C*H=CH_2), 128.6, 128.6, 128.6, 128.5, 128.0, 128.0, 127.9, 127.8, 127.8 (CH_{Arom}), 117.2 (CH_2-CH=*CH_2*) 82.6 (C-4), 81.3 (C-2), 79.6 (C-3), 75.4 (CH_2Bn), 75.0, 73.5 (C-5), 73.4, 73.4 (CH_2Bn), 72.2 (C-1), 66.1 (C-6), 36.4 (*CH_2*-CH=CH_2). HRMS (ESI) [M/Z]: [M + NH_4] calcd for $C_{37}NH_{44}O_5^+$ 582.3266 found 582.3216. Spectral data for the β-anomer: ^{1}H NMR (400 MHz, $CDCl_3$, HH-COSY, HSQC, HMBC, HMBC-GATED) δ 7.39 – 7.20 (m, 20H, CH_{Arom}), 5.71 (dddd, *J* = 16.6, 10.2, 7.7, 6.2 Hz, 1H, CH_2-C*H*=CH_2), 5.02 (dq, *J* = 17.2, 1.6 Hz, 1H, CH_2-CH=C*H*H), 4.97 (ddt, *J* = 10.2, 2.3, 1.2 Hz, 1H, CH_2-CH=C*H*H), 4.74 – 4.65 (m, 2H, 2x CH*H*Bn), 4.57 (dd, *J* = 12.1, 4.1 Hz, 2H, 2x CH*H*Bn), 4.54 – 4.46 (m, 2H, 2x CH*H*Bn), 4.35 – 4.25 (m, 2H, 2x CH*H*Bn), 3.92 (td, *J* = 6.1, 1.8 Hz, 1H, H-5), 3.72 – 3.67 (m, 2H, H-1 H-6), 3.64 – 3.58 (m, 2H, H-3 H-6), 3.40 – 3.36 (m, 1H, H-4), 3.21 – 3.17 (m, 1H, H-2), 2.61 – 2.51 (m, 1H, CH*H*-CH=CH_2), 2.29 – 2.20 (m, 1H, CH*H*-CH=CH_2). ^{13}C NMR (101 MHz, $CDCl_3$, HSQC, HMBC, HMBC-GATED) δ 138.3, 138.0 (C_q), 135.4 (CH_2-*C*H=CH_2), 128.9, 128.8, 128.6, 128.4, 128.1, 128.0, 128.0, 128.0, 127.9, 127.6 (CH_{Arom}), 116.8 (CH_2-CH=*CH_2*), 76.1 (C-1), 75.8 (C-5), 73.6 (CH_2 Bn), 73.4 (C-2), 72.5 (CH_2 Bn), 72.4 (C-4), 72.3 (CH_2 Bn), 72.0 (CH_2 Bn), 70.2 (C-3), 70.0 (C-6), 35.5 (*CH_2*-CH=CH_2). HRMS (ESI) [M/Z]: [M + NH_4] calcd for $C_{37}NH_{44}O_5^+$ 582.3266 found 582.3217.

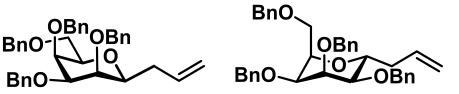

1-allyl-1-deoxy-2,3,4,6-tetra-*O*-benzyl-D-talopyranoside (S8). The title compound was prepared according to the general glycosylation procedure, using talose donor **8**[22] and allyl(chloro)dimethylsilane (0.058 mmol, 33 mg, 58%, >98:2, α:β) or allyltrimethylsilane (0.037 mmol, 21 mg, 37%, 63:37, α:β) or allyltributylstannane (0.043 mmol, 24 mg, 43%, 18:82, α:β), yielding the title compound as a colorless oil. Spectral data for the α-anomer: ^{1}H NMR (400 MHz, $CDCl_3$, HH-COSY, HSQC, HMBC, HMBC-GATED) δ 7.40 – 7.21 (m, 20H, CH_{Arom}), 5.89 (dddd, *J* = 17.5, 10.2, 7.6, 6.3 Hz, 1H, CH_2-CH=CH_2), 5.14 – 5.03 (m, 2H, CH_2-CH=CH_2), 4.78 – 4.68 (m, 2H, CH_2Bn), 4.62 – 4.48 (m, 5H, 5x CH*H* Bn), 4.36 (d, *J* = 11.6 Hz, 1H, CH*H* Bn), 4.32 (td, *J* = 6.9, 3.5 Hz, 1H, H-5), 4.16 (dd, *J* = 11.9, 8.8 Hz, 1H, H-6), 4.12 (t, *J* = 2.5 Hz, 1H, H-3), 3.92 (ddd, *J* = 10.3, 7.0, 3.1 Hz, 1H, H-1), 3.80 (dd, *J* = 12.0, 1.9 Hz, 1H, H-6), 3.60 (dd, *J* = 6.3, 2.4 Hz, 1H, H-4), 3.12 (dd, *J* = 9.4, 2.7 Hz, 1H, H-2), 2.64 – 2.54 (m, 1H, CH*H*-CH=CH_2), 2.28 – 2.18 (m, 1H, CH*H*-CH=CH_2). ^{13}C NMR (101 MHz, $CDCl_3$, HSQC, HMBC, HMBC-GATED) δ 135.03 (CH_2-CH=CH_2), 128.6, 128.5, 128.4, 128.3, 128.0, 127.9, 127.9, 127.9, 127.6, 127.5, 127.5 (CH_{Arom}), 117.1 (CH_2-CH=CH_2), 78.1 (C-2), 77.0 (C-4), 75.2 (C-5), 74.0 (CH_2Bn), 73.3 (CH_2Bn), 73.16 (C-3), 71.4 (CH_2Bn), 71.1 (CH_2Bn), 67.5 (C-1), 66.4 (C-6), 35.9 (CH_2-CH=CH_2). HRMS (ESI) [M/Z]: [M + NH_4] calcd for $C_{37}NH_{44}O_5^+$ 582.3266 found 582.3216. Spectral data for the β-anomer: ^{1}H NMR (400 MHz, $CDCl_3$, HH-COSY, HSQC, HMBC, HMBC-GATED) δ 7.40 – 7.20 (m, 20H, CH_{Arom}), 5.71 (dddd, *J* = 16.8, 10.2, 7.7, 6.3 Hz, 1H, CH_2-C*H*=CH_2), 5.06 – 4.90 (m, 4H, CH_2-CH=CH_2 2x CH*H*Bn), 4.81 (dd, *J* = 13.3, 11.9 Hz, 2H, 2x CH*H*Bn), 4.60 (d, *J* = 4.5 Hz, 2H, 2x CH*H*Bn), 4.49 (d, *J* = 16.6 Hz, 1H, CH*H*Bn), 3.93 (dd, *J* = 3.0, 1.5 Hz, 1H, H-3), 3.76 – 3.72 (m, 1H, H-2), 3.69 (dd, *J* = 6.1, 1.4 Hz, 2H, 2x H-6), 3.52 (td, *J* = 6.1, 1.5 Hz, 1H, H-5), 3.48 (t, *J* = 3.0 Hz, 1H, H-4), 3.29 (ddd, *J* = 7.6, 6.4, 1.4 Hz, 1H, H-1), 2.59 (dddt, *J* = 13.9, 7.7, 6.3, 1.5 Hz, 1H, CH*H*-CH=CH_2), 2.32 (dddt, *J* = 14.3, 7.6, 6.4, 1.2 Hz, 1H, CH*H*-CH=CH_2). ^{13}C NMR (101 MHz, $CDCl_3$, HSQC, HMBC, HMBC-GATED) δ 135.1 (CH_2-*C*H=CH_2), 128.7, 128.6, 128.6, 128.6, 128.4, 128.2, 128.2, 128.1, 127.5, 127.4, 127.3 (CH_{Arom}), 117.1 (CH_2-CH=*C*H_2), 82.3 (C-4), 80.0 (C-1), 79.1 (C-5), 74.3, 74.2, 74.0 (CH_2Bn), 74.0 (C-2), 73.7 (CH_2Bn), 72.8 (C-3), 71.0 (CH_2Bn), 69.9 (C-6), 35.9 (*C*H_2-CH=CH_2). HRMS (ESI) [M/Z]: [M + NH_4] calcd for $C_{37}NH_{44}O_5^+$ 582.3266 found 582.3210.

References

(1) Crich, D.; Sharma, I. Is Donor–Acceptor Hydrogen Bonding Necessary for 4,6-*O*-Benzylidene-Directed β-Mannopyranosylation? Stereoselective Synthesis of β-*C*-Mannopyranosides and α-*C*-Glucopyranosides. *Org. Lett.* **2008**, *10* (21), 4731–4734. https://doi.org/10.1021/ol8017038.

(2) Moumé-Pymbock, M.; Crich, D. Stereoselective C-Glycoside Formation with 2-*O*-Benzyl-4,6-*O*-Benzylidene Protected 3-Deoxy Gluco- and Mannopyranoside Donors: Comparison with *O*-Glycoside Formation. *J. Org. Chem.* **2012**, *77* (20), 8905–8912. https://doi.org/10.1021/jo3011655.

(3) McGarvey, G. J.; LeClair, C. A.; Schmidtmann, B. A. Studies on the Stereoselective Synthesis of C-Allyl Glycosides. *Org. Lett.* **2008**, *10* (21), 4727–4730. https://doi.org/10.1021/ol801710s.

(4) Paulsen, H.; Trautwein, W.-P.; Espinosa, F. G.; Heyns, K. Carboxoniumverbindungen in der Kohlenhydratchemie, III. Einfache Synthese von D-Idose aus D-Glucose durch mehrfache Acetoxonium-Ion-Umlagerungen. Darstellung eines stabilen Acetoxonium-Salzes der Tetraacetyl-idose. *Chem. Ber.* **1967**, *100* (9), 2822–2836. https://doi.org/10.1002/cber.19671000908.

(5) Bock, K.; Sommer, M. B. A Simplified Synthesis of Penta-*O*-Acetyl-α-D-Altropyranose. *Acta Chem. Scand.* **1980**, 389.

(6) Dinkelaar, J.; van den Bos, L. J.; Hogendorf, W. F. J.; Lodder, G.; Overkleeft, H. S.; Codée, J. D. C.; van der Marel, G. A. Stereoselective Synthesis of L-Guluronic Acid Alginates. *Chem. Eur. J.* **2008**, *14* (30), 9400–9411. https://doi.org/10.1002/chem.200800960.

(7) Wang, Q.; Fu, J.; Zhang, J. A Facile Preparation of Peracylated α-Aldopyranosyl Chlorides with Thionyl Chloride and Tin Tetrachloride. *Carbohydr. Res.* **2008**, *343* (17), 2989–2991. https://doi.org/10.1016/j.carres.2008.08.037.

(8) Walvoort, M. T. C.; Moggré, G.-J.; Lodder, G.; Overkleeft, H. S.; Codée, J. D. C.; van der Marel, G. A. Stereoselective Synthesis of 2,3-Diamino-2,3-Dideoxy-β-D-Mannopyranosyl Uronates. *J. Org. Chem.* **2011**, *76* (18), 7301–7315. https://doi.org/10.1021/jo201179p.

(9) Hansen, T.; Lebedel, L.; Remmerswaal, W. A.; van der Vorm, S.; Wander, D. P. A.; Somers, M.; Overkleeft, H. S.; Filippov, D. V.; Désiré, J.; Mingot, A.; Bleriot, Y.; van der Marel, G. A.; Thibaudeau, S.; Codée, J. D. C. Defining the S_N1 Side of Glycosylation Reactions: Stereoselectivity of Glycopyranosyl Cations. *ACS Cent. Sci.* **2019**, *5* (5), 781–788. https://doi.org/10.1021/acscentsci.9b00042.

(10) Mayr, H.; Kempf, B.; Ofial, A. R. π-Nucleophilicity in Carbon–Carbon Bond-Forming Reactions. *Acc. Chem. Res.* **2003**, *36* (1), 66–77. https://doi.org/10.1021/ar020094c.

(11) Ammer, J.; Nolte, C.; Mayr, H. Free Energy Relationships for Reactions of Substituted Benzhydrylium Ions: From Enthalpy over Entropy to Diffusion Control. *J. Am. Chem. Soc.* **2012**, *134* (33), 13902–13911. https://doi.org/10.1021/ja306522b.

(12) Mayr, H.; Bug, T.; Gotta, M. F.; Hering, N.; Irrgang, B.; Janker, B.; Kempf, B.; Loos, R.; Ofial, A. R.; Remennikov, G.; Schimmel, H. Reference Scales for the Characterization of Cationic Electrophiles and Neutral Nucleophiles. *J. Am. Chem. Soc.* **2001**, *123* (39), 9500–9512. https://doi.org/10.1021/ja010890y.

(13) Remmerswaal, W. A.; Hansen, T.; Hamlin, T. A.; Codée, J. D. C. Origin of Stereoselectivity in S_E2' Reactions of Six-Membered Ring Oxocarbenium Ions. *Chem. Eur. J.* **2023**, *29* (14), e202203490. https://doi.org/10.1002/chem.202203490.

(14) Fu, Y.; Bernasconi, L.; Liu, P. Ab Initio Molecular Dynamics Simulations of the S_N1/S_N2 Mechanistic Continuum in Glycosylation Reactions. *J. Am. Chem. Soc.* **2021**, *143* (3), 1577–1589. https://doi.org/10.1021/jacs.0c12096.

(15) The TS-α-$^0S_2$ transition states for both glycosyl cations could not be identified by conventional means due to electronic instability of the associated reactant complexes. As a representative structure for the transition state geometry, the point on the associated constrained potential energy surface with a similar C•••Si bond stretch as the TS-α-$^4C_1$ was selected. Supplementary Figures S1 and S2 contain diagrams which contain the Δ*E* along the reaction coordinate of each reaction pathway, demonstrating how this representative structure was selected. To demonstrate the effectiveness of this method, the reaction profiles between the glycosyl cations and allyltrichlorosilane were computed. For this weaker nucleophile the TS-α-$B_{2,5}$ transition states are clearly defined. In Supplementary Figures S3 and S4, it can be observed how the TS-α-$B_{2,5}$ barrier height compares with the other reaction paths.

(16) Frisch, M. J.; Trucks, G. W.; Cheeseman, J. R.; Scalmani, G.; Caricato, M.; Hratchian, H. P.; Li, X.; Barone, V.; Bloino, J.; Zheng, G.; Vreven, T.; Montgomery, J. A.; Petersson, G. A.; Scuseria, G. E.; Schlegel, H. B.; Nakatsuji, H.; Izmaylov, A. F.; Martin, R. L.; Sonnenberg, J. L.; Peralta, J. E.; Heyd, J. J.; Brothers, E.; Ogliaro, F.; Bearpark, M.; Robb, M. A.; Mennucci, B.; Kudin, K. N.; Staroverov, V. N.; Kobayashi, R.; Normand, J.; Rendell, A.; Gomperts, R.; Zakrzewski, V. G.; Hada, M.; Ehara, M.; Toyota, K.; Fukuda, R.; Hasegawa, J.; Ishida, M.; Nakajima, T.; Honda, Y.; Kitao, O.; Nakai, H. Gaussian 09 Rev. D.01, 2009.

(17) Becke, A. D. Density-functional Thermochemistry. III. The Role of Exact Exchange. *J. Chem. Phys.* **1993**, *98* (7), 5648–5652. https://doi.org/10.1063/1.464913.

(18) Lee, C.; Yang, W.; Parr, R. G. Development of the Colle-Salvetti Correlation-Energy Formula into a Functional of the Electron Density. *Phys. Rev. B Condens. Matter* **1988**, *37* (2), 785–789. https://doi.org/10.1103/physrevb.37.785.
(19) Vosko, S. H.; Wilk, L.; Nusair, M. Accurate Spin-Dependent Electron Liquid Correlation Energies for Local Spin Density Calculations: A Critical Analysis. *Can. J. Phys.* **1980**, *58* (8), 1200–1211. https://doi.org/10.1139/p80-159.
(20) Ditchfield, R.; Hehre, W. J.; Pople, J. A. Self-Consistent Molecular-Orbital Methods. IX. An Extended Gaussian-Type Basis for Molecular-Orbital Studies of Organic Molecules. *J. Chem. Phys.* **1971**, *54* (2), 724–728. https://doi.org/10.1063/1.1674902.
(21) Bootsma, A. N.; Wheeler, S. Popular Integration Grids Can Result in Large Errors in DFT-Computed Free Energies. ChemRxiv July 29, 2019. https://doi.org/10.26434/chemrxiv.8864204.v5.
(22) Hengst, J. M. A. van. Structure-Reactivity Relationships in Glycosylation Chemistry, Leiden University, 2023.